frontiers

Nonlinear Dendritic Coincidence Detection for Supervised Learning

Fabian Schubert [1,*] **and Claudius Gros** [1]

[1] *Institute for Theoretical Physics, Goethe University Frankfurt am Main, Germany*

Correspondence*:
Institute for Theoretical Physics
Goethe University Frankfurt am Main
Max-von-Laue-Str. 1
60438 Frankfurt am Main, Germany
fschubert@itp.uni-frankfurt.de

ABSTRACT

Cortical pyramidal neurons have a complex dendritic anatomy, whose function is an active field of scientific research. In particular, the segregation between its soma and the apical dendritic tree is believed to play an active role in processing feed-forward sensory information and top-down or feedback signals. In this work, we use a simple two-compartment model accounting for the nonlinear interactions between basal and apical input streams and show that a simple Hebbian learning rule in the basal compartment allows the neuron to align its basal input to a target signal in the apical compartment. We show that this learning process, termed coincidence detection, is robust against strong distractions in the basal input space and demonstrate its effectiveness in a linear classification task.

Keywords: Dendrites, Pyramidal Neuron, Plasticity, Coincidence Detection, Supervised Learning

1 INTRODUCTION

In recent years, a growing body of research has addressed the functional implications of the distinct physiology and anatomy of cortical pyramidal neurons (Spruston, 2008; Hay et al., 2011; Ramaswamy and Markram, 2015). In particular, on the theoretical side, we saw a paradigm shift from treating neurons as point-like electrical structures towards embracing the entire dendritic structure (Larkum et al., 2009; Poirazi, 2009; Shai et al., 2015a). This was mostly due to the fact that experimental work uncovered dynamical properties of pyramidal neuronal cells that simply could not be accounted for by point models (Spruston et al., 1995; Häusser et al., 2000).

An important finding is that the apical dendritic tree of cortical pyramidal neurons can act as a separate nonlinear synaptic integration zone (Spruston, 2008; Branco and Häusser, 2011). Under certain conditions, a dendritic Ca^{2+} spike can be elicited that propagates towards the soma, causing rapid, bursting spiking activity. One of the cases in which dendritic spiking can occur was termed 'backpropagation-activated Ca^{2+} spike firing' ('BAC firing'): A single somatic spike can backpropagate towards the apical spike initiation zone, in turn significantly facilitating the initiation of a dendritic spike (Stuart and Häusser, 2001; Spruston, 2008; Larkum, 2013). This reciprocal coupling is believed to act as a form of coincidence detection: If apical and basal synaptic input co-occurs, the neuron can respond with a rapid burst of spiking activity. The firing rate of these temporal bursts exceeds the firing rate that is maximally achievable under basal

synaptic input alone, therefore representing a form of temporal coincidence detection between apical and basal input.

Naturally, these mechanisms also affect plasticity and thus learning within the cortex (Sjöström and Häusser, 2006; Ebner et al., 2019). While the interplay between basal and apical stimulation and its effect on synaptic efficacies is subject to ongoing research, there is evidence that BAC-firing tends to shift plasticity towards long-term potentiation (LTP) (Letzkus et al., 2006). Thus, coincidence between basal and apical input appears to also gate synaptic plasticity.

In a supervised learning scheme, where the top down input arriving at the apical compartment acts as the teaching signal, the most straight-forward learning rule for the basal synaptic weights would be derived from an appropriate loss function, such as a mean square error, based on the difference between basal and apical input, i.e. $I_p - I_d$, where indices p and d denote 'proximal' and 'distal', in equivalence to basal and apical. Theoretical studies have investigated possible learning mechanisms that could utilize an intracellular error signal (Urbanczik and Senn, 2014; Schiess et al., 2016; Guerguiev et al., 2017). However, a clear experimental evidence for a physical quantity encoding such an error is—to our knowledge—yet to be found. On the other hand, Hebbian-type plasticity is extensively documented in experiments (Gustafsson et al., 1987; Debanne et al., 1994; Markram et al., 1997; Bi and Poo, 1998). Therefore, our work is based on the question whether the non-linear interactions between basal and apical synaptic input could, when combined with a Hebbian plasticity rule, allow a neuron to learn to reproduce an apical teaching signal in its proximal input.

We investigate coincidence learning by combining a phenomenological model that generates the output firing rate as a function of two streams of synaptic input (subsuming basal and apical inputs) with Hebbian, as well as BCM-like plasticity rules on basal synapses. In particular we hypothesized that this combination of neural activation and plasticity rules would lead to an increased correlation between basal and apical inputs. Furthermore, the temporal alignment observed in our study could potentially facilitate apical inputs to act as top-down teaching signals, without the need for an explicit error-driven learning rule. Thus, we also test our model in a simple linear supervised classification task and compare it with the performance of a simple point neuron equipped with similar plasticity rules.

2 MODEL

2.1 Neuron Model

The neuron model used throughout this study is a discrete-time rate encoding model that contains two separate input variables, subsuming the total synaptic input current injected arriving at the basal (proximal) and apical (distal) dendritic structure of a pyramidal neuron, respectively. The model is a slightly simplified version of a phenomenological model proposed by Shai et al. (2015b). Denoting the input currents I_p (proximal) and I_d (distal), the model is written as

$$\begin{aligned} y\left(t\right) = &\alpha\sigma\left(I_p(t) - \theta_{p0}\right)\left[1 - \sigma\left(I_d(t) - \theta_d\right)\right] \\ &+ \sigma\left(I_d(t) - \theta_d\right)\sigma\left(I_p(t) - \theta_{p1}\right) \end{aligned} \tag{1}$$

$$\sigma(x) \equiv \frac{1}{1 + \exp(-4x)}\,. \tag{2}$$

Here, $\theta_{p0} > \theta_{p1}$ and θ_d are threshold variables with respect to proximal and distal inputs. Overall, equation (1) describes two distinct regions of neural activation in the (I_p, I_d)-space which differ in their maximal firing rates, which are set to 1 and α, where $0 < \alpha < 1$. A plot of (1) is shown in Fig. 1.

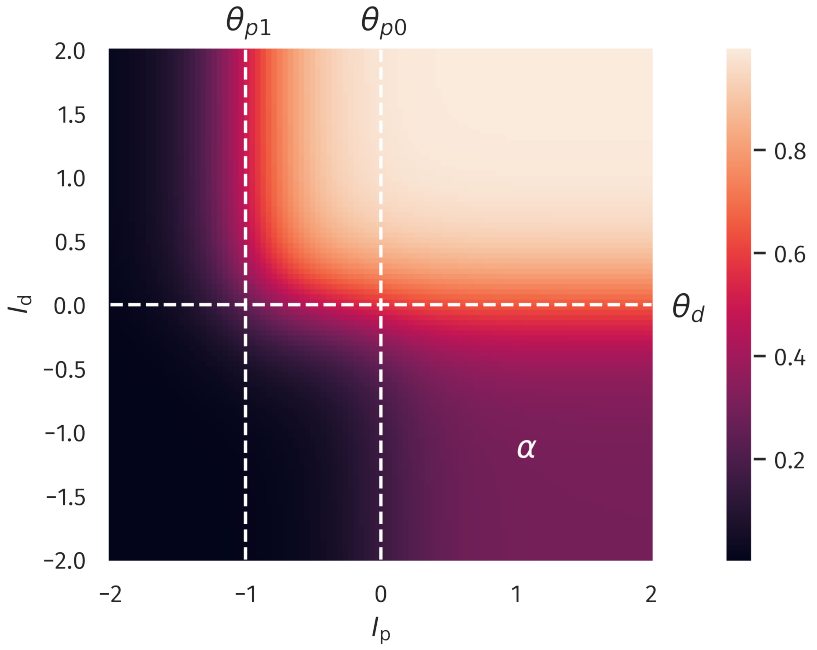

Figure 1. Two-compartment rate model. The firing rate as a function of proximal and distal inputs I_p and I_d, see (1). The thresholds θ_{p0}, θ_{p1} and θ_d define two regions of neural activity, with a a maximal firing rate of unity an a plateau at $\alpha = 0.3$.

When both input currents I_d and I_p are large, viz larger than the thresholds θ_d and θ_{p1}, the second term in (1) dominates, which leads to $y \approx 1$. An intermediate activity plateau, of strength α emerges in addition when $I_p > \theta_{p0}$ and $I_d < \theta_d$. As such, the compartment model (1) is able to distinguish neurons with a normal activity level, here encoded by $\alpha = 0.3$, and strongly bursting neurons, where the maximal firing rate is unity. The intermediate plateau allows neurons to process the proximal inputs I_p even in the absence of distal stimulation. The distal current I_d acts therefore as an additional modulator.

In our numerical experiments we compare the compartment model with a classical point neuron, as given by

$$y(t) = \sigma\left(I_p(t) + I_d(t) - \theta\right) \ . \tag{3}$$

The apical input I_d is generated 'as is', meaning, it is not dynamically calculated as a superposition of multiple presynaptic inputs. To be concrete, we used

$$I_d(t) = n_d(t)x_d(t) - b_d(t) \ , \tag{4}$$

where $n_d(t)$ is a scaling factor, $x_d(t)$ a pre-generated discrete time sequence and $b_d(t)$ a bias. Note that n_d and b_d are time dependent since they are subject to adaptation processes, which will be described in the next section. Similarly, the proximal input $I_p(t)$ is given by

$$I_p(t) = n_p(t) \sum_{i=1}^{N} x_{p,i}(t) w_i(t) - b_p(t) \ , \tag{5}$$

where N is the number of presynaptic afferents, $x_{p,i}(t)$ the corresponding sequences, $w_i(t)$ the synaptic efficacies and $n_p(t)$ and $b_p(t)$ the (time dependent) scaling and bias. Tyical values for the parameters used throughout this study are presented Table 1.

2.2 Plasticity

We implemented a Hebbian plasticity rule for the proximal synaptic weights by the following update equation:

$$w_i(t+1) = w_i(t) + \mu_w \left(x_{p,i}(t) - \tilde{x}_{p,i}(t)\right)\left(y(t) - \tilde{y}\right) \tag{6}$$

$$\tilde{x}_{p,i}(t+1) = (1-\mu_{\text{av}})\tilde{x}_{p,i}(t) + \mu_{\text{av}} x_{p,i}(t) \tag{7}$$

$$\tilde{y}(t+1) = (1-\mu_{\text{av}})\tilde{y}(t) + \mu_{\text{av}} y(t) \tag{8}$$

The trailing time averages $\tilde{x}_{p,i}$ and $\tilde{y}$, respectively of the presynaptic basal activites, $x_{p,i}$, and of the neural firing rate y, enter the Hebbian learing rule (6) as reference levels. Pre- and post-synaptic neurons are considered to be active/inactive when being above/below the respective trailing averages. The timescale of the averaging, $1/\mu_{\text{av}}$, is typcially over 200 time steps, see Table 1. With $1/\mu_w = 2 \cdot 10^4$ learning is assumed to be be considerably slower, as usual for statistical update rules. Additionally, we use a synaptic normalization constraint,

$$w_i(t) \to \frac{w_i(t)}{\|\mathbf{w}(t)\|} \ , \tag{9}$$

in each time step, where $\|\mathbf{w}(t)\|$ denotes the Euclidean norm of the synaptic weight vector. For comparative reasons, the point neuron model is equipped with the same plasticity rule for the proximal weights as (6).

The bias variables entering the definitions (4) and (5) of the distal proximal currrent, I_d and I_p, are assumed to adapt accodingly to

$$b_p(t+1) = b_p(t) + \mu_b \left[I_p(t) - I_p^t\right] \tag{10}$$

$$b_d(t+1) = b_d(t) + \mu_b \left[I_d(t) - I_d^t\right] \ , \tag{11}$$

where $I_p^t = 0$ and, $I_d^t = 0$ are preset targets and $1/\mu_b = 10^3$ the timescale for the adaption process. Over time, both the distal and the proximal currents, I_d and I_p, average out.

Adaption rules for the bias entering a transfer function, such as (11) and (10), have the task to regulate overall activitiy levels. The overall magnitude of the synaptic weights, which are determined by synaptic rescaling factors, here n_d and n_p, as defined in (4) and (5), will regulate in contrast the variance of the

Table 1. Model parameters, as defined in sections 2.1 and 2.2.

θ_{p0}	0	V_d^t	0.25
θ_{p1}	-1	μ_b	10^{-3}
θ_d	0	μ_n	10^{-4}
α	0.3	μ_{av}	$5 \cdot 10^{-3}$
μ_w	$5 \cdot 10^{-5}$	I_p^t	0
V_p^t	0.25	I_d^t	0

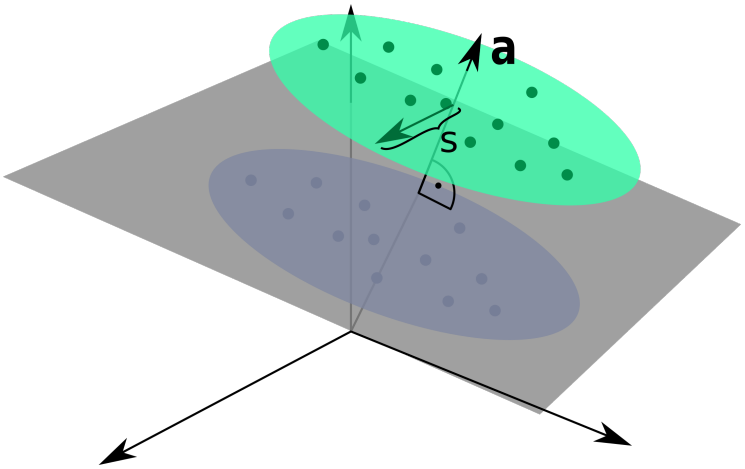

Figure 2. Input Space for the Linear Classification Task. Two clusters of presynaptic basal activities were generated from multivariate Gaussian distributions. Here, s denotes the standard deviation orthogonal to the normal vector $\mathbf{a}$ of the classification hyperplane, as defined by (16).

neural activity, and not the average level (Schubert and Gros, 2021). In this spirit we consider

$$n_d(t+1) = n_d(t) + \mu_n \left[V_d^t - \left(I_d(t) - \tilde{I}_d(t) \right)^2 \right] \tag{12}$$

$$n_p(t+1) = n_p(t) + \mu_n \left[V_p^t - \left(I_p(t) - \tilde{I}_p(t) \right)^2 \right] \tag{13}$$

$$\tilde{I}_d(t+1) = (1-\mu_{\text{av}})\tilde{I}_d(t) + \mu_{\text{av}} I_d(t) \tag{14}$$

$$\tilde{I}_p(t+1) = (1-\mu_{\text{av}})\tilde{I}_p(t) + \mu_{\text{av}} I_p(t) \tag{15}$$

Here, V_p^t and V_p^t define targets for the temporal averaged variances of I_p and I_d. The dynamic variables $\tilde{I}_p$ and $\tilde{I}_d$ are simply low-pass filtered running averages of I_p and I_d. Overall, the framework specified here allows the neuron to be fully flexible, as long as the activtiy level and its variance fluctuate around preset target values (Schubert and Gros, 2021). A list of the parameter values used throughout this investigation is given in Table 1. Our choices of target means and variances are based on the assumption that neural input should be tuned towards a certain working regime of the neural transfer function. In the case of the presented model, this means that both proximal and distal input cover an area where the nonlinearities of the transfer function are reflected without oversaturation.

3 RESULTS

3.1 Alignment between Basal and Apical Inputs

As a first test, we quantify the neuron's ability to align its basal input to the apical teaching signal. This can be done using the pearson correlation coefficient $\rho[I_p, I_d]$ between the basal and apical input currents. We determined $\rho[I_p, I_d]$ after the simulation, which involves all plasticity mechanisms, both for the synaptic weights and for the intrinsic parameters. The input sequences $x_{p,i}(t)$ is randomly drawn from a uniform distribution, in $[0, 1]$, which is done independently for each $i \in [1, N]$.

For the distal current $I_d(t)$ to be fully 'reconstructable' by the basal input, $x_d(t)$ has to be a linear combination

$$x_d(t) = \sum_{i=1}^{N} a_i x_{p,i}(t) \tag{16}$$

of the $x_{p,i}(t)$, where the a_i are the components of a random vector $\mathbf{a}$ of unit length.

Given that we use with (6) a Hebbian learning scheme, one can expect that the direction and the magnitude of the principal components of the basal input may affect the outcome of the simulation significantly: A large variance in the basal input orthogonal to the 'reconstruction vector' $\mathbf{a}$ is a distraction for the plasticity. The observed temporal alignment between I_p and I_d should hence suffer when such a distraction is present. The situaton is illustrated in Fig. 2.

In order to test the effects of distracting directions, we applied a transformation to the input sequences $x_{p,i}(t)$. For the transformation two parameters are used, a scaling factor s and the dimension N_{dist} of the distracting subspace within the basal input space. The N_{dist} randomly generated basis vectors are orthogonal to the superposition vector $\mathbf{a}$, as defined by (16), and to each others. Within this N_{dist}-dimensional subspace, the input sequences $x_{p,i}(t)$ are rescaled subsequently by the factor s. See Fig. 2. After the learning phase, a second set of input sequences $x_{p,i}(t)$ and $x_d(t)$ is generated for testing purposes, using the identical protocol, and the cross correlation $\rho[I_p, I_d]$ evaluated. During the testing phase plasticity is turned off.

The overall aim of our portocal is to evaluate the degree $\rho[I_p, I_d]$ to which the proximal current I_p aligns in the temporal domain to the distal input I_d. We recall that this is a highly non-trivial question, given that the proximal synpatic weights are adapted via Hebbian plasticity, see (6). The error $(I_p - I_d)^2$ does not enter the adaption rules employed. Results are presented in Fig. 3 as a function of the distraction parameters s and $N_{\text{dist}} \in [0, N-1]$. The total number of basal inputs is $N = 100$.

For a comparison, in Fig. 3 data for both the compartment model and for a point neuron are presented, as defined respectively by (1) and (3). One can observe a decorrelation transition for both models. However, the compartment model supports a significantly stronger distraction in terms of the scaling factor s as compared to the point model. This is a first confirmation of our hypothesis that nonlinear interactions between basal and apical input could improve learning guided by top-down signals.

3.2 Supervised Learning in a Linear Classification Task

Next, we investigated if the observed differences would also improve the performance in an actual supervised learning task. For this purpose, we constructed presynaptic basal input as illustrated in Fig. 2. Written in vector form, each sample from the basal input is generated from the following expression:

$$\mathbf{x}_p(t) = \mathbf{b} + \mathbf{a}\left(c(t) + \sigma_a \zeta_a(t)\right) + s \cdot \sum_{i=1}^{N_{\text{dist}}} \zeta_{dist,i}(t) \mathbf{v}_{dist,i} \ . \tag{17}$$

Here, $\mathbf{b}$ is a random vector drawn uniformly from $(0,1)^N$, $\mathbf{a}$ is random unit vector as introduced in Section 3.1, $c(t)$ is a binary variable drawn from $\{-0.5, 0.5\}$ with equal probability and $\zeta_a(t)$ and the $\zeta_{dist,i}(t)$ are independent random Gaussian variables with zero mean and unit variance. Hence, σ_a simply denotes the standard deviation of each Gaussian cluster along the direction of the normal vector $\mathbf{a}$ and was set to $\sigma_a = 0.25$. Finally, the set of $\mathbf{v}_{dist,i}$ forms a randomly generated orthogonal basis of N_{dist} unit vectors which—just as in Section 3.1—are also orthogonal to $\mathbf{a}$. The free parameter s parameterized the

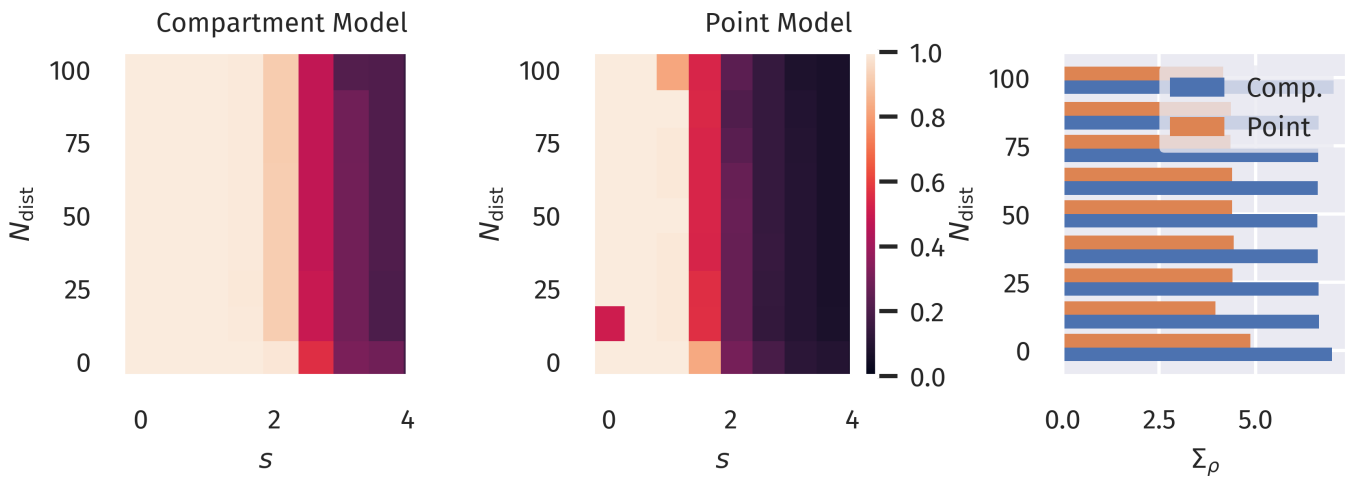

Figure 3. Alignment between Basal and Apical Input. Color encoded the Pearson correlation $\rho[I_p, I_d]$ between the proximal and distal input currents, I_p and I_d. Data for a range of the orthogonal distraction directions, $N_{\text{dist}} \in [0, N-1]$, and the scaling factor s, as defined in Fig. 2. The overall number of basal inputs is $N = 100$. The quantity Σ_ρ depicted in the bar plot is the sum over all correlation values for the different tested values of s under a given N_{dist}. Blue bar represents the compartment model, orange the point model.

standard deviation along this subspace orthogonal to $\mathbf{a}$. As indicated by the time dependence, the Gaussian and binary random variables are drawn for each time step. The vectors $\mathbf{b}$, $\mathbf{a}$, and $\mathbf{v}_{dist,i}$ are generated once before the beginning of a simulation run.

For the classification task, we set up two output neurons receiving the same basal presynaptic input, while the top-down input encoded the correct linear classification in a one-hot scheme, that is

$$x_{d,0}(t) = 1 - \Theta\left((\mathbf{x}_p(t) - \mathbf{b})^T \mathbf{a}\right) \tag{18}$$

$$x_{d,1}(t) = \Theta\left((\mathbf{x}_p(t) - \mathbf{b})^T \mathbf{a}\right) \ , \tag{19}$$

where $\Theta(x)$ is the Heaviside step function.

As in the previous experiment, we ran a full simulation until all dynamic variables reached a stationary state. After this, a test run without plasticity and with the apical input turned off was used to evaluate the classification performance. For each sample, the index of the neuron with the highest activity was used as the predicted class. Accuracy was then calculated as the fraction of correctly classified samples.

The resulting accuracy as a function of N_{dist} and s is shown in Fig. 4. Albeit differences are small, the compartment model does show a better overall accuracy for the tested parameter range. It should be noted, though, that the advantage of the compartment model becomes even less prominent when looking at the actual correlation between proximal and distal input as a measure of successful learning (as done in the previous section). Fig. 8 in the supplementary section shows that the compartment model allows for a marginally larger scaling among the distraction dimensions.

3.3 Non-Hebbian Learning Rules

Instead of Hebbian learning, we also considered a BCM-like learning rule for the basal weights (Bienenstock et al., 1982; Intrator and Cooper, 1992). The form of the BCM-rule we consider here

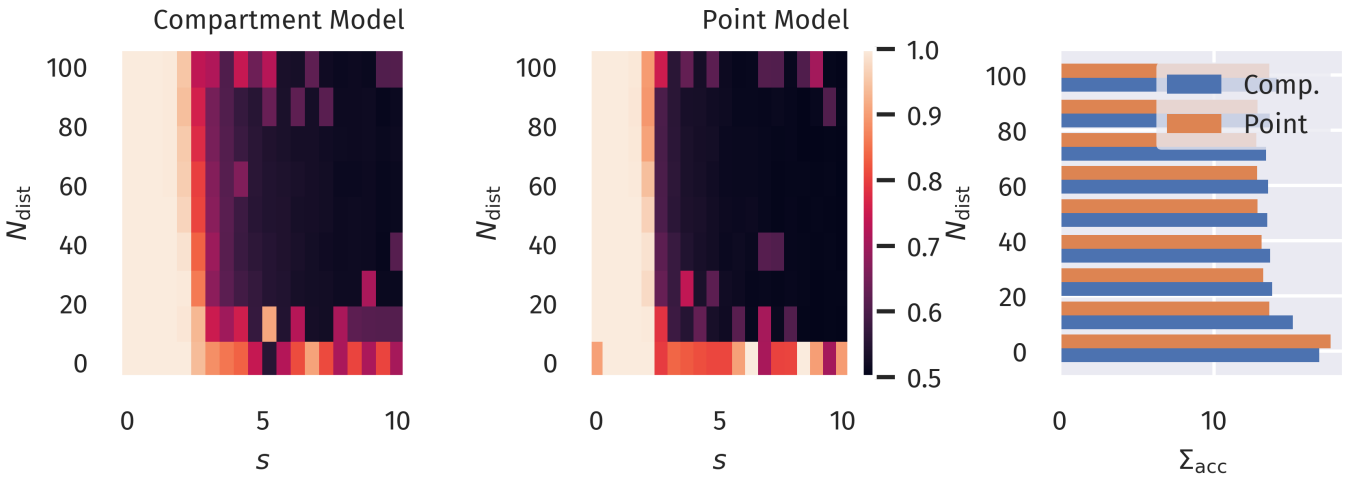

Figure 4. Binary Classification Accuracy. Fraction of correctly classified patterns as illustrated in Fig. 2, see Section 3.2. The quantity Σ_{acc} depicted in the bar plot is the sum over all accuracies for the different tested values of s under a given N_{dist}. Blue bar represents the compartment model, orange the point model.

reads

$$\Delta w_i \propto y\,(y - \theta_M)\,x_i - \epsilon w_i \ , \tag{20}$$

where θ_M is a threshold defining a transition from LTP to LTD and ϵ is an optional decay term on the weights. In the variant introduced by Law and Cooper (1994), the sliding threshold is simply the temporal average of the squared neural activity, $\theta_M = \langle y^2 \rangle$. In practice, this would be calculated as a running average, thereby preventing the weights from growing indefinitely.

However, for our compartment model, we chose to explicitly set the threshold to be the mean value between the high- and low-activity regime in our compartment model, i.e. $\theta_M = (1+\alpha)/2$. By doing so, LTP is preferably induced if both basal and apical input are present at the same time. Furthermore, instead of the weight decay term, we chose to keep the weight normalization as introduced in (9). Obviously, for the point model, the reasoning behind our choice of θ_M did not apply. Still, to provide some level of comparability, we also ran simulations with a point model where the sliding threshold was calculated as a running average of y^2. Furthermore, we did not use weight normalization in this case, but chose to use a small weight decay term with $\epsilon = 0.1$. The results are shown in Fig. 5 (classification task) and Fig. 5 (Basal-Apical alignment). While the accuracy of the classification for the point model is at most comparable to Hebbian learning, the BCM-like rule for the compartment model significantly increases the accuracy for the tested parameter range (compare Fig. 4). Still, as for the Hebbian learning rule, this result should be taken with a grain of salt, as Fig. 9 in the supplementary section indicates that a rather large part of the region ($s > 5$) showing good classification performance for the compartment model in Fig. 5 does hardly exhibit any actual correlation between proximal and distal input, making it likely that the accuracy of the classification could be easily impaired in this regime, e.g. by injecting small amounts of noise.

The compartment model also significantly benefits from the BCM rule in terms of basal-apical alignment as tested in Sect. 3.1, while only marginal improvements can be observed for the point model (compare Fig. 6 with Fig. 3).

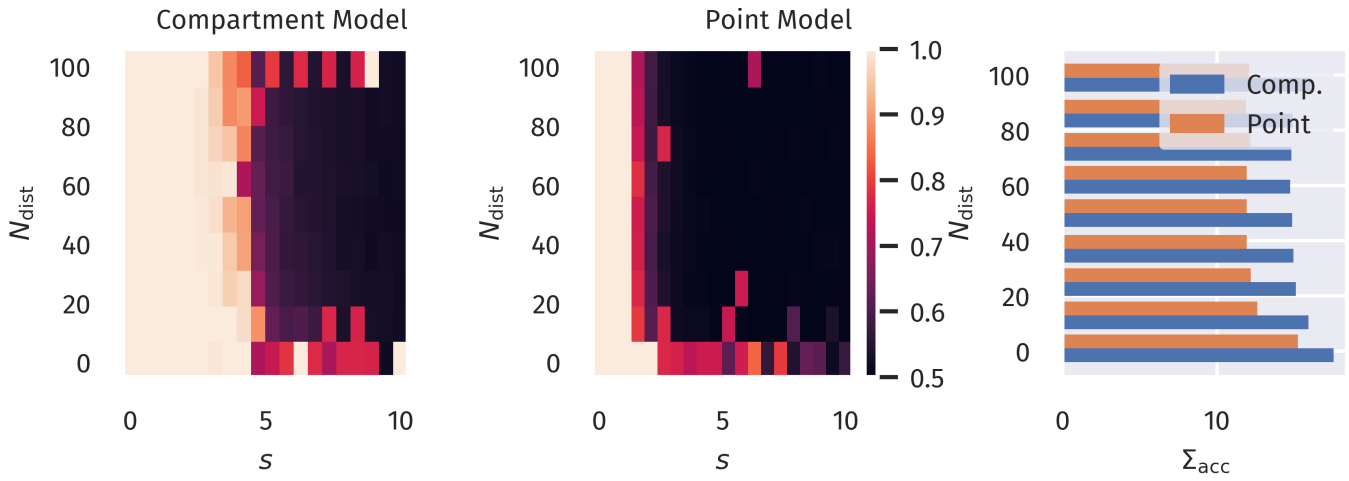

Figure 5. Binary Classification Accuracy, BCM Rule. Fraction of correctly classified patterns as illustrated in Fig. 2, after training with a BCM-like learning rule. The quantity Σ_{acc} depicted in the bar plot is the sum over all accuracies for the different tested values of s under a given N_{dist}. Blue bar represents the compartment model, orange the point model.

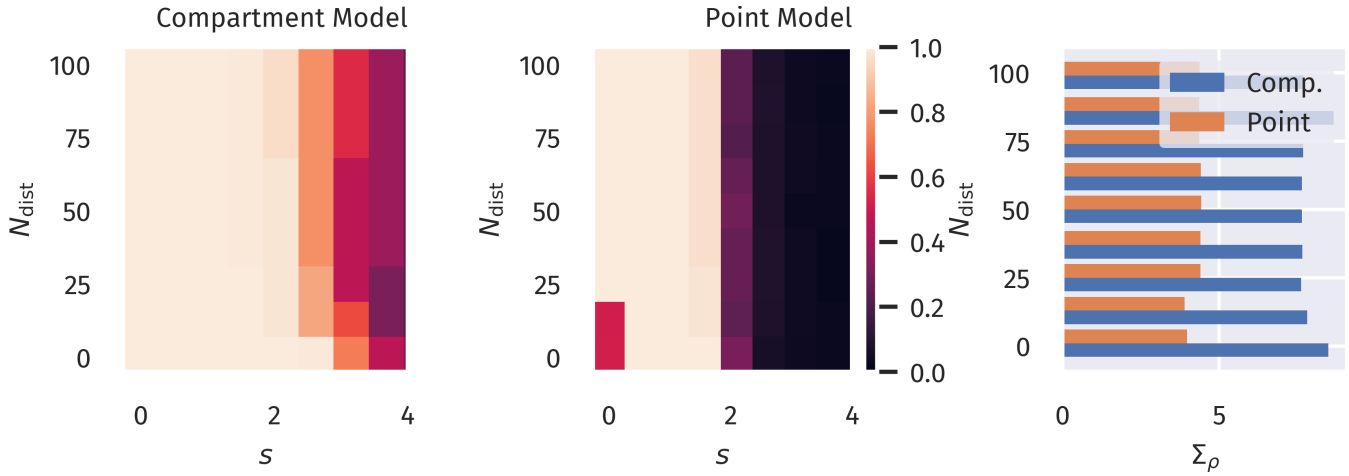

Figure 6. Alignment between Basal and Apical Input, BCM Rule. Color encodes the Pearson correlation $\rho[I_p, I_d]$ for different number of orthogonal distraction directions N_{dist} and the corresponding scaling faction s after training with a BCM-like rule. The quantity Σ_{ρ} depicted in the bar plot is the sum over all correlation values for the different tested values of s under a given N_{dist}. Blue bar represents the compartment model, orange the point model. Compare to Fig. 3.

3.4 Objective Function of BCM Learning in the Compartment Model

To form a better understanding of why the BCM-type learning rule in combination with the implemented compartment model, we can formalize the learning rule for the proximal weights in terms of an objective function. For this purpose, we further simplify (1) by replacing the sigmoid functions $\sigma(x)$ by a simple step function $\Theta(x)$. This does not change the overall shape or topology of the activation in the (I_p, I_d) space but merely makes the smooth transitions sharp and instantaneous. Using $\Delta w_i \propto y\,(y-\theta_M)\,x_i$, we find in this case

$$\begin{aligned}\Delta w_i \propto\ &[(1-\alpha)\Theta(I_d-\theta_d)\Theta(p-\theta_{p1})\\ &+\alpha(\alpha-1)\Theta(\theta_d-I_d)\Theta(p-\theta_{p0})]x_i\ .\end{aligned} \tag{21}$$

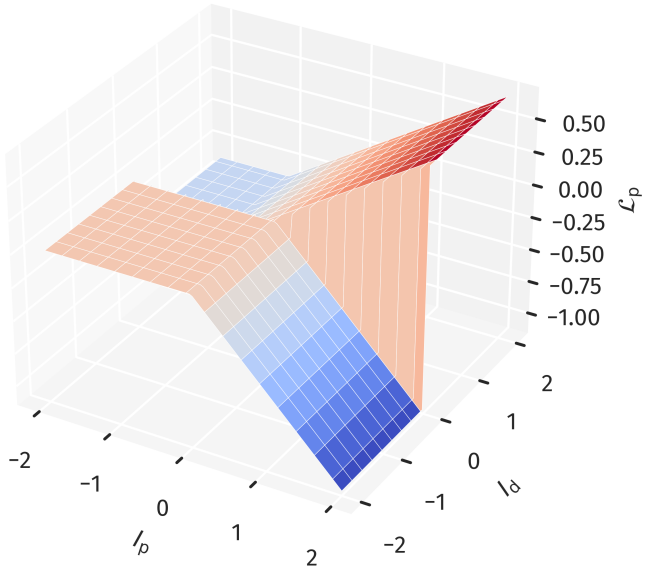

Figure 7. Objective Function for the Proximal Weight Update. The approximate objective function for the proximal weights as given in (23). This corresponds to a combination of using (1) together with (20). Note the ridge-like structure along the I_p-I_d diagonal, which supports the alignment between proximal and distal input.

Noting that $\Theta(x)$ is the first derivative of the ReLu function $[x]^+ \equiv \max(0, x)$, we find that this update rule can be written as

$$\Delta w_i \propto \frac{\partial \mathcal{L}_p}{\partial w_i} \tag{22}$$

$$\begin{aligned} \mathcal{L}_p \equiv\ & (1-\alpha)\Theta(I_d - \theta_d)[p - \theta_{p1}]^+ \\ & + \alpha(\alpha - 1)\Theta(\theta_d - I_d)[p - \theta_{p0}]^+ \ . \end{aligned} \tag{23}$$

The objective function is shown in Fig. 7. One can observe that states closer to the I_p-I_d diagonal are preferred, while the opposite is the case for off-diagonal states. This provides an explanation why the BCM-rule can induce an alignment between proximal and distal inputs when used in combination with the nonlinear compartment model.

It should be noted, though, that to a certain extent, the objective function is not scale-invariant (as would be e.g. if the squared error was used) in the sense that the prior distributions of both proximal and distal inputs need a certain mean and variance to cover a region of input states for which the described effects can take place. As a counterexample, one could imagine that the input samples only covered a flat of $\mathcal{L}_p$, as for example in Fig. 7 on the left, leading to a zero average gradient. This is prevented, however, by the homeostatic processes acting simultaneously on the gains and biases.

4 DISCUSSION

We have demonstrated that in a simple supervised learning scheme, the proposed two-compartment transfer function significantly increases the robustness of the learning process against distracting components in the proximal input space. This was most prominently found when combined with a BCM-like learning rule.

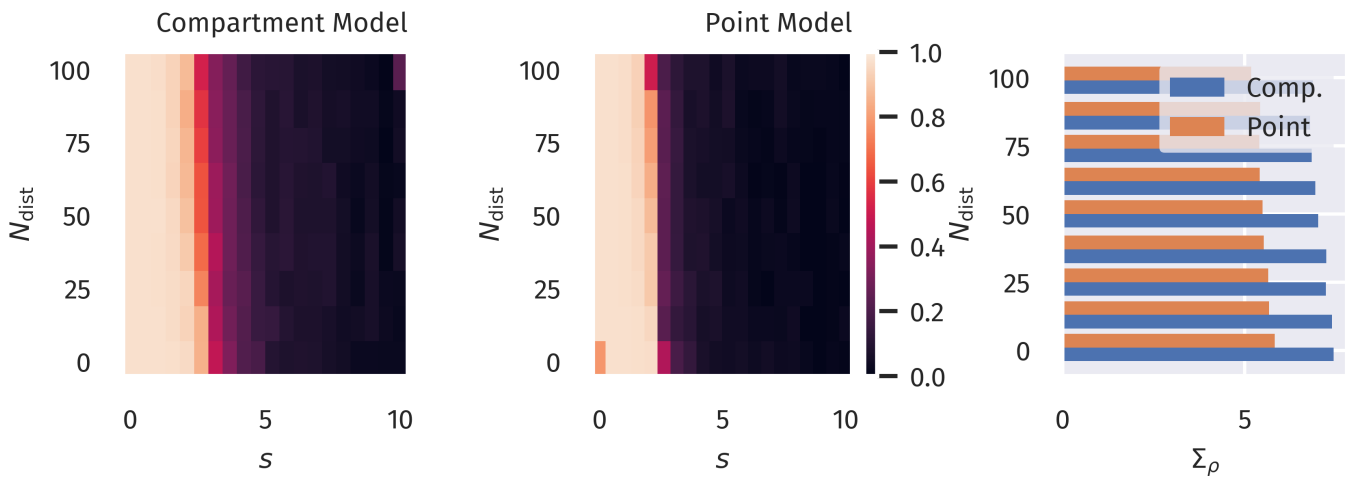

Figure 8. Alignment between Basal and Apical Input after Binary Classification Learning. Correlation between proximal and distal Input after training as described in Sect. 3.2. The quantity Σ_ρ depicted in the bar plot is the sum over all correlation values for the different tested values of s under a given N_{dist}. Blue bar represents the compartment model, orange the point model.

The idea of target-backpropagation in multi-layered networks has already been proposed in different variants (Bengio, 2014; Lee et al., 2015; Guerguiev et al., 2017). Yet, all of these approaches assume a learning rule being dependent on an explicit error term between top-down and bottom up signals guiding plasticity in some form or another. In this work, we considered an alternative approach, that is, the correlation between proximal and distal input as a maximization objective, in combination with homeostatic adaptation rules that regulate proximal and distal inputs into a desired "working regime", see Sect. 3.4. Since I_p is a linear projection of the proximal input space, maximizing the correlation between I_p and I_d can be regarded as a form of canonical correlation analysis (CCA) (Härdle and Simar, 2007). The idea of investigating CCA as a possible mode of synaptic learning has previously been investigated by Haga and Fukai (2018). Interestingly, according to the authors, a BCM-learning term in the plasticity dynamics accounts for principal component analysis in the input space, while CCA requires an additional multiplicative term between local basal and apical activity. In contrast, our results indicate that such a multiplicative term is not required to drive basal synaptic plasticity towards a maximal alignment between basal and apical input, even in the presence of distracting principal components. Apart from the advantage that this avoids the necessity of giving a biophysical interpretation of such cross-terms, it is also in line with the view that synaptic plasticity should be formulated in terms of local membrane voltage traces (Clopath et al., 2010; Weissenberger et al., 2018). Distal compartments then only implicitly affect plasticity, e.g. by facilitating spike initiation.

As we did not include higher-dimensional distal input patterns, it remains an open question how target signals would be formed in multi-layered network structures. However, as previous works have indicated, random top-down weights can be sufficient for successful credit assignment and learning (Lillicrap et al., 2016; Guerguiev et al., 2017). Therefore, our results could potentially also be transferred to deeper network structures, where plasticity is guided by local errors between top-down and bottom-up signals.

5 SUPPLEMENTARY MATERIAL

CONFLICT OF INTEREST STATEMENT

The authors declare that the research was conducted in the absence of any commercial or financial relationships that could be construed as a potential conflict of interest.

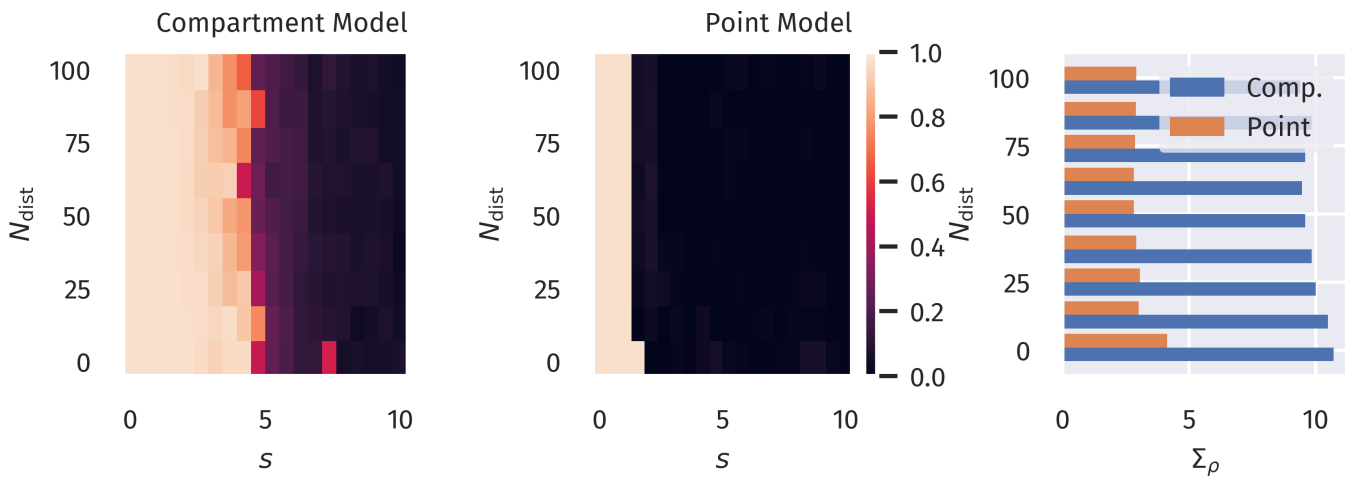

Figure 9. Alignment between Basal and Apical Input after Binary Classification Learning using a BCM-like Rule. Correlation between proximal and distal Input after linear classification training as described in Sect. 3.2, but using the plasticity rules given in Sect. 3.3. The quantity Σ_ρ depicted in the bar plot is the sum over all correlation values for the different tested values of s under a given N_{dist}. Blue bar represents the compartment model, orange the point model.

AUTHOR CONTRIBUTIONS

Both authors, F.S. and C.G., contributed equally to the writing and review of the manuscript. F.S. provided the code, ran the simulations and prepared the figures.

ACKNOWLEDGMENTS

The authors acknowledge the financial support of the German research foundation (DFG)

DATA AVAILABILITY STATEMENT

The datasets [GENERATED/ANALYZED] for this study can be found in the [NAME OF REPOSITORY] [LINK].

REFERENCES

Bengio, Y. (2014). How Auto-Encoders Could Provide Credit Assignment in Deep Networks via Target Propagation

Bi, G. Q. and Poo, M. M. (1998). Synaptic modifications in cultured hippocampal neurons: Dependence on spike timing, synaptic strength, and postsynaptic cell type. *Journal of Neuroscience* 18, 10464–10472. doi:10.1523/jneurosci.18-24-10464.1998

Bienenstock, E. L., Cooper, L. N., and Munro, P. W. (1982). Theory for the development of neuron selectivity: Orientation specificity and binocular interaction in visual cortex. *Journal of Neuroscience* 2, 32–48. doi:10.1523/jneurosci.02-01-00032.1982

Branco, T. and Häusser, M. (2011). Synaptic Integration Gradients in Single Cortical Pyramidal Cell Dendrites. *Neuron* 69, 885–892. doi:10.1016/j.neuron.2011.02.006

Clopath, C., Büsing, L., Vasilaki, E., and Gerstner, W. (2010). Connectivity reflects coding: A model of voltage-based STDP with homeostasis. *Nature Neuroscience* 13, 344–352. doi:10.1038/nn.2479

Debanne, D., Gähwiler, B. H., and Thompson, S. M. (1994). Asynchronous pre- and postsynaptic activity induces associative long-term depression in area CA1 of the rat hippocampus in vitro. *Proceedings of*

the National Academy of Sciences of the United States of America 91, 1148–1152. doi:10.1073/pnas.91.3.1148

Ebner, C., Clopath, C., Jedlicka, P., and Cuntz, H. (2019). Unifying Long-Term Plasticity Rules for Excitatory Synapses by Modeling Dendrites of Cortical Pyramidal Neurons. *Cell Reports* 29, 4295–4307.e6. doi:10.1016/j.celrep.2019.11.068

Guerguiev, J., Lillicrap, T. P., and Richards, B. A. (2017). Towards deep learning with segregated dendrites. *eLife* 6. doi:10.7554/eLife.22901

Gustafsson, B., Wigstrom, H., Abraham, W. C., and Huang, Y. Y. (1987). Long-term potentiation in the hippocampus using depolarizing current pulses as the conditioning stimulus to single volley synaptic potentials. *Journal of Neuroscience* 7, 774–780. doi:10.1523/jneurosci.07-03-00774.1987

Haga, T. and Fukai, T. (2018). Dendritic processing of spontaneous neuronal sequences for single-trial learning. *Scientific Reports* 8, 15166. doi:10.1038/s41598-018-33513-9

Härdle, W. and Simar, L. (2007). Canonical Correlation Analysis. In *Applied Multivariate Statistical Analysis* (Berlin, Heidelberg: Springer Berlin Heidelberg). 321–330. doi:10.1007/978-3-540-72244-1_14

[Dataset] Häusser, M., Spruston, N., and Stuart, G. J. (2000). Diversity and dynamics of dendritic signaling. doi:10.1126/science.290.5492.739

Hay, E., Hill, S., Schürmann, F., Markram, H., and Segev, I. (2011). Models of Neocortical Layer 5b Pyramidal Cells Capturing a Wide Range of Dendritic and Perisomatic Active Properties. *PLoS Computational Biology* 7, e1002107. doi:10.1371/journal.pcbi.1002107

Intrator, N. and Cooper, L. N. (1992). Objective function formulation of the BCM theory of visual cortical plasticity: Statistical connections, stability conditions. *Neural Networks* 5, 3–17. doi:10.1016/S0893-6080(05)80003-6

[Dataset] Larkum, M. (2013). A cellular mechanism for cortical associations: An organizing principle for the cerebral cortex. doi:10.1016/j.tins.2012.11.006

Larkum, M. E., Nevian, T., Sandier, M., Polsky, A., and Schiller, J. (2009). Synaptic integration in tuft dendrites of layer 5 pyramidal neurons: A new unifying principle. *Science* 325, 756–760. doi:10.1126/science.1171958

Law, C. C. and Cooper, L. N. (1994). Formation of receptive fields in realistic visual environments according to the Bienenstock, Cooper, and Munro (BCM) theory. *Proceedings of the National Academy of Sciences of the United States of America* 91, 7797–7801. doi:10.1073/pnas.91.16.7797

Lee, D. H., Zhang, S., Fischer, A., and Bengio, Y. (2015). Difference target propagation. In *Lecture Notes in Computer Science (including subseries Lecture Notes in Artificial Intelligence and Lecture Notes in Bioinformatics)* (Springer Verlag), vol. 9284, 498–515. doi:10.1007/978-3-319-23528-8_31

Letzkus, J. J., Kampa, B. M., and Stuart, G. J. (2006). Learning Rules for Spike Timing-Dependent Plasticity Depend on Dendritic Synapse Location. *Journal of Neuroscience* 26, 10420–10429. doi:10.1523/JNEUROSCI.2650-06.2006

Lillicrap, T. P., Cownden, D., Tweed, D. B., and Akerman, C. J. (2016). Random synaptic feedback weights support error backpropagation for deep learning. *Nature Communications* 7, 1–10. doi:10.1038/ncomms13276

Markram, H., Lübke, J., Frotscher, M., and Sakmann, B. (1997). Regulation of synaptic efficacy by coincidence of postsynaptic APs and EPSPs. *Science* 275, 213–215. doi:10.1126/science.275.5297.213

Poirazi, P. (2009). Information processing in single cells and small networks: Insights from compartmental models. In *AIP Conference Proceedings* (American Institute of Physics), vol. 1108, 158–167. doi:10.1063/1.3117124

[Dataset] Ramaswamy, S. and Markram, H. (2015). Anatomy and physiology of the thick-tufted layer 5 pyramidal neuron. doi:10.3389/fncel.2015.00233

Schiess, M., Urbanczik, R., and Senn, W. (2016). Somato-dendritic Synaptic Plasticity and Error-backpropagation in Active Dendrites. *PLoS Computational Biology* 12, 1004638. doi:10.1371/journal.pcbi.1004638

Schubert, F. and Gros, C. (2021). Local homeostatic regulation of the spectral radius of echo-state networks. *Frontiers in computational neuroscience* 15, 12

Shai, A. S., Anastassiou, C. A., Larkum, M. E., and Koch, C. (2015a). Physiology of Layer 5 Pyramidal Neurons in Mouse Primary Visual Cortex: Coincidence Detection through Bursting. *PLOS Computational Biology* 11

Shai, A. S., Anastassiou, C. A., Larkum, M. E., and Koch, C. (2015b). Physiology of Layer 5 Pyramidal Neurons in Mouse Primary Visual Cortex: Coincidence Detection through Bursting. *PLOS Computational Biology* 11

Sjöström, P. J. and Häusser, M. (2006). A Cooperative Switch Determines the Sign of Synaptic Plasticity in Distal Dendrites of Neocortical Pyramidal Neurons. *Neuron* 51, 227–238. doi:10.1016/j.neuron.2006.06.017

Spruston, N. (2008). Pyramidal neurons: dendritic structure and synaptic integration. *Nature Reviews Neuroscience* 9, 206–221. doi:10.1038/nrn2286

Spruston, N., Schiller, Y., Stuart, G., and Sakmann, B. (1995). Activity-dependent action potential invasion and calcium influx into hippocampal CA1 dendrites. *Science* 268, 297–300. doi:10.1126/science.7716524

Stuart, G. J. and Häusser, M. (2001). Dendritic coincidence detection of EPSPs and action potentials. *Nature Neuroscience* 4, 63–71. doi:10.1038/82910

Urbanczik, R. and Senn, W. (2014). Learning by the Dendritic Prediction of Somatic Spiking. *Neuron* 81, 521–528. doi:10.1016/j.neuron.2013.11.030

Weissenberger, F., Gauy, M. M., Lengler, J., Meier, F., and Steger, A. (2018). Voltage dependence of synaptic plasticity is essential for rate based learning with short stimuli. *Scientific Reports* 8, 4609. doi:10.1038/s41598-018-22781-0